materials

MDPI

Article

312 MAX Phases: Elastic Properties and Lithiation

P.P. Filippatos [1,2], M.A. Hadi [3], S.-R.G. Christopoulos [1], A. Kordatos [1], N. Kelaidis [1], M.E. Fitzpatrick [1], M. Vasilopoulou [2] and A. Chroneos [1,4,*]

1 Faculty of Engineering, Environment and Computing, Coventry University, Priory Street, Coventry CV1 5FB, UK; filippap@uni.coventry.ac.uk (P.P.F.); ac0966@coventry.ac.uk (S.-R.G.C.); ap.kordatos@gmail.com (A.K.); ad1978@coventry.ac.uk (N.K.); ab6856@coventry.ac.uk (M.E.F.)
2 Institute of Nanoscience and Nanotechnology (INN), National Center for Scientific Research "Demokritos", AgiaParaskevi, 15341 Athens, Greece; m.vasilopoulou@inn.demokritos.gr
3 Department of Physics, University of Rajshahi, Rajshahi 6205, Bangladesh; hadipab@gmail.com
4 Department of Materials, Imperial College London, London SW7 2BP, UK
* Correspondence: alexander.chroneos@imperial.ac.uk or ab8104@coventry.ac.uk

Received: 25 October 2019; Accepted: 3 December 2019; Published: 8 December 2019

Abstract: Interest in the $M_{n+1}AX_n$ phases (M = early transition metal; A = group 13–16 elements, and X = C or N) is driven by their ceramic and metallic properties, which make them attractive candidates for numerous applications. In the present study, we use the density functional theory to calculate the elastic properties and the incorporation of lithium atoms in the 312 MAX phases. It is shown that the energy to incorporate one Li atom in Mo_3SiC_2, Hf_3AlC_2, Zr_3AlC_2, and Zr_3SiC_2 is particularly low, and thus, theoretically, these materials should be considered for battery applications.

Keywords: MAX phases; DFT; elastics; lithiation

1. Introduction

MAX phases are a class of ternary nitrides and carbides that we can categorize into families of $M_{(n+1)}AX_n$, with n = 1, 2, 3, 4, and other MAX phase-related structures like the 321 MAX phases or the iMAX phases [1–4]. A family of 211 of these materials was discovered in powder form in 1960, with the name H-phases from Nowotny et al. [5], but, after many years, Barsoum and El-Taghy synthesized the first bulk MAX phase, Ti_3SiC_2 [6], with enough purity to enable them to characterize its properties. Since then, there interest has grown regarding MAX compounds, due to their unusual properties, which are a result of their bonding characteristics and their structures [7–14]. Just like MXenes, which are the corresponding binary carbides and nitrides that are created from MAX phases after an exfoliation process that removes the A layer [7], the MAX compounds have a high elastic stiffness and are good electrical conductors [8]. Regarding their mechanical behavior, MAX phases are machinable and have high thermal and damage resistance [11,12]. These properties have constituted the 312 MAX phases as important materials for numerous high-end applications, including space, electronic, and nuclear [13–25].

A schematic of the crystal structure ($P6_3/mmc$, space group no. 194) [5] of the 312 MAX phases is given in Figure 1. The "metallic" layers (A) are positioned between the n "ceramic" layers (M_3AX_2 for n = 2) along the c-direction. The M and X layers effectively form M_2X slabs, with face-centered cubic-type stacking. In the present research, we have examined the potential application of the 312 MAX phases as anode materials in Li-ion batteries or supercapacitors. Modern battery technology uses the 3D carbon structure, graphite, as an anode material, and there are reports that graphene batteries that could have better performances [26]. Etching the A from the MAX compounds leads to the 2D material MXenes, which, from a theoretical point, could become the future Li-ion battery anode material, as it exhibits better cycles than graphite [27,28]. However, in order to create the MXenes, the method of

hydrofluoric acid (HF) etching is used, and although it removes the A layer, it also affects the bonding between the M and X layers. This creates some unwanted characteristic changes, as it sometimes affects the elastic properties of the material. Moreover, although in most cases MXenes have unique electrical characteristics, sometimes when the etching removes the A layer, the resulting structure becomes a semiconductor [29], and as a result, this MXene cannot be used as an anode material. Recently, the first 2D MAX phases (MAXenes) were demonstrated that consist of a 2D structure, which, unlike the 2D MXenes, keeps the A layer [30]. In order to examine the application of MAXenes in Li-ion batteries, it is evident that the interactions of Li in the MAX phases should be examined first in order to predict how the lithiation is affected by the A layer. Lastly, as has been indicated in previous studies, the creation of MXenes is a high-cost method [29]. From all of the above, we believe that our research is important, as the Li-doped MAX phases could have better performances in the Li-ion batteries technology than MXenes, and moreover, they have never been investigated before.

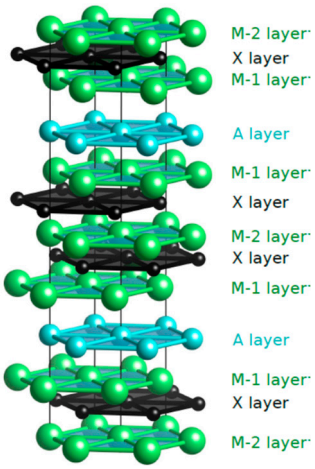

Figure 1. Crystal structure of the 312 MAX phase.

The aim of the present work is to study the elastic properties and Li formation in the M_3AX_2 phases (M = Hf, Nb, Ta, Ti, V, Zr, and Mo; A = Si, Al, Sn, Ga, and In; X = C) using the density functional theory (DFT), and to compare our results with other related experimental and theoretical studies. Although Mo_3SiC_2, Hf_3AlC_2, Zr_3AlC_2, and Zr_3SiC_2 are of interest, it should be noted that not all of these compounds have been synthesized yet, although there are many reports that provide some of them in stable forms. Specifically, Zhou et al. [31] have synthesized an Zr_3AlC_2 together with Solvas-Zapata et al. [32], who synthesized $Zr_3(Al_{1-x}Si_x)C_2$. Regarding Mo_3SiC_2, there are many theoretical reports [33] about its properties, like self-healing. However, it has not been synthesized. There are also experimental reports on stable forms of Zr_3SnC_2 and Hf_3AlC_2 from Lapauw et al. [34]. There are also some trends in thin film MAX phases [35], as well as in sol-gel methods of creating the MAX phases compounds [36], that are examined by experimentalists for the synthesis of new MAX phases. To conclude, of the four 312 materials that we propose should be examined for potential lithiation, two of them have already been synthesized in stable forms (Zr_3SnC_2 and Hf_3AlC_2) and one has been synthesized as part of a mixed structure (Zr_3SiC_2); accordingly, we believe that their lithiation abilities could be investigated both experimentally and theoretically. We will then propose some experimental works with the stable synthesized forms of the 312 MAX phases that could be examined, in order to see their performances as Li-ion battery anodes.

2. Computational Methods

CASTEP, a plane-wave DFT code, was employed for all the calculations [37,38]. The generalized gradient approximation, ultra-soft pseudopotentials [39], and the Purdew, Burke, and Ernzerhof (PBE) [40] exchange-correlation function were used. To optimize the geometry,

the Broyden–Fletcher–Goldfarb–Shanno (BFGS) minimizer was employed and implemented in the CASTEP. The supercells contained 108 atomic sites, with a plane-wave basis set cut-off of 450 eV, 3 × 3 × 1 Monkhorst–Pack (MP) [41]. The Li interstitial was placed at all possible sites. After an extensive search for all the possible sites, we found all the minimum energy positions of the Li interstitials. The minimum energy sites are presented in Figure 2. For the elastic properties, a unit cell was considered, with a plane-wave energy cut-off of 550 eV and with 18 × 18 × 2*k*-point mesh.

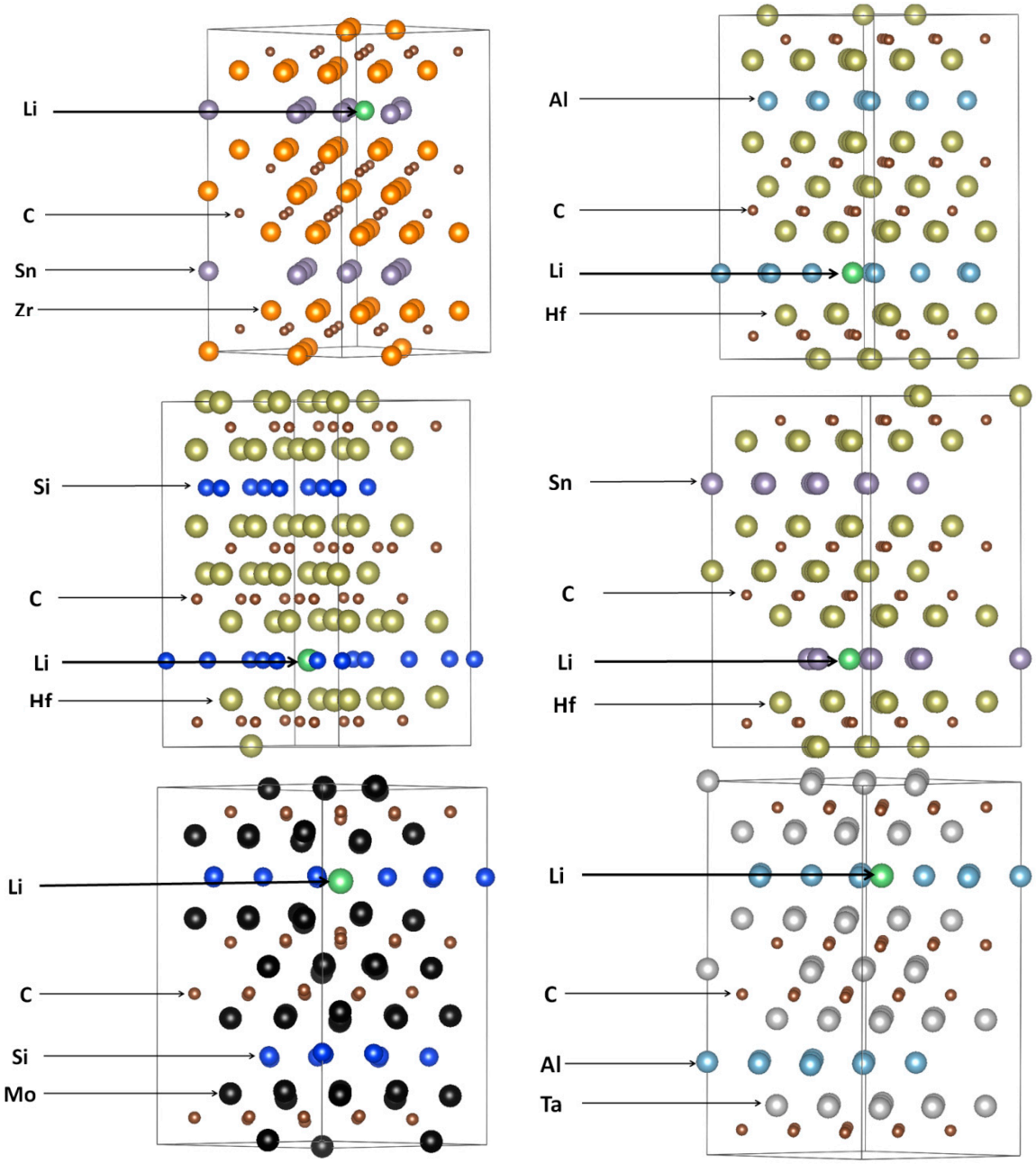

Figure 2. *Cont.*

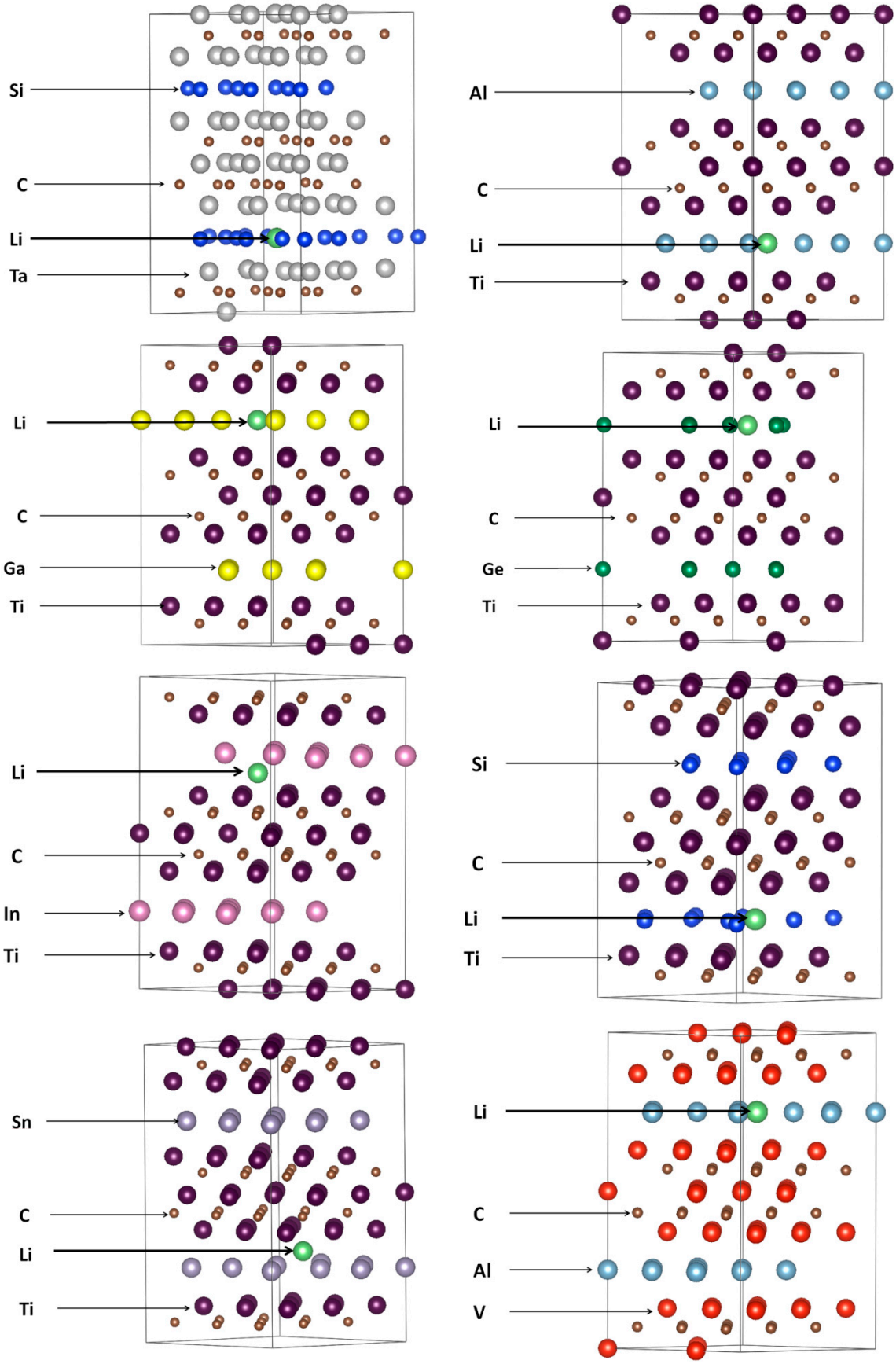

Figure 2. *Cont.*

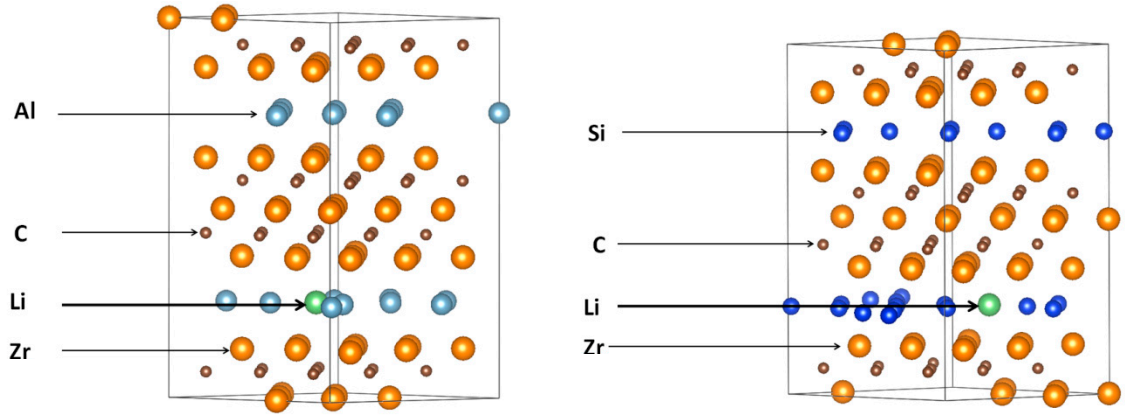

Figure 2. The Li interstitial positions (green atoms) in the 312 MAX phases.

3. Results

3.1. Elastic Properties

The mechanical behavior of materials is dependent on their elastic constants. Moreover, the elastic properties of the materials are linked to the bonding characteristics, so the information that the elastic constants provide is also connected to the chemical bonds of the atoms of the solid. The MAX compounds have hexagonal crystal structures [5,42]. Therefore, the 312 MAX phases have six different elastic constants: c_{11}, c_{12}, c_{13}, c_{33}, c_{44}, and c_{66}. Only the first five of them are independent, taking into account that $c_{66} = (c_{11} - c_{12})/2$. In order for the MAX compounds to be dynamically stable, the following conditions must be met [43]:

$$c_{11} > 0, c_{33} > 0, c_{44} > 0, (c_{11} + c_{12})\, c_{33} > 2(c_{13})^2, \text{and } (c_{11} - c_{12}) > 0 \quad (1)$$

The calculated results for the selected 312 MAX phases have been investigated in previous studies [44,45]. In Table 1, we present the elastic properties of the 312 MAX phases. It is seen that the above conditions are met, and so the studied MAX phases are mechanically stable.

The elastic stiffness of a solid, regarding the (100) <100> strain, is calculated by the c_{11} constant. Thus, V_3AlC_2 is the stiffest. On the other hand, Zr_3AlC_2 and Ti_3InC_2 are the least stiff. The c_{12} elastic constant is a measure of the deformation of the material in the (110) plane along the <100> direction. Therefore, Ti_3AlC_2 is the most easily deformed. The c_{12} and c_{13} values indicate that when force is applied along the a- crystallographic axis, Ti_3AlC_2, Ti_3InC_2, Ti_3GaC_2, and V_3AlC_2 are easier to shear along the b and c axes than the other MAX compounds in Table 1. Lastly, the lower value of c_{33} for Zr_3SnC_2 results in the conclusion that it is easiest to deform via <001> compression under uniaxial stress.

Focusing on the bulk elastic parameters, in Table 1, the bulk modulus B, Young's modulus Y, and the shear modulus G have been calculated. It is evident that the Zr_3SnC_2 has the lowest value of B, and, as a consequence, it has the lowest resistance under compression. Conversely, Mo_3SiC_2, which has the highest value, has the highest resistance to compression. The shear modulus G has the lowest value in Zr_3SnC_2, and so this MAX phase is more prone to shape change than the others. The Young's modulus Y, which is a measure of the stress required for deformation, has the lowest value in the Zr_3SnC_2 MAX phase, compared to the other MAX phases in Table 1 (also refer to [44–52]).

Table 1. Calculated elastic constants Cij (GPa), bulk modulus B (GPa), shear modulus G (GPa), Young's modulus Y (GPa), Poisson's ratio v, Pugh's ratio B/G, elastic anisotropy factor A, and shear anisotropy factor (kc/ka) for the 312 MAX phases *. Comparison with previous studies [44–52].

Phase	c_{11}	c_{12}	c_{13}	c_{33}	c_{44}	A	k_c/k_a	B	G	Y	B/G	v	Ref.
Ti_3AlC_2	355	74	66	295	125	0.971	1.314	157	131	307	1.199	0.174	[44]
	358	84	75	293	122	0.974	1.343	163	127	303	1.279	0.190	[47]
	361	75	70	299	124	0.954	1.297	160	131	309	1.221	0.178	[47]
	368	81	76	313	130	0.983	1.253	168	135	320	1.245	0.183	[46]
	-	-	-	-	-	-	-	165	124	297	1.331	0.20	[49]
Zr_3AlC_2	322	84	97	287	138	1.330	1.116	165	122	294	1.353	0.203	This
	314	78	79	262	107	1.024	1.279	151	110	266	1.373	0.207	[46]
V_3AlC_2	404	84	108	361	158	1.151	1.075	197	153	364	1.288	0.191	This
	390	82	116	358	158	1.225	0.991	196	147	354	1.333	0.200	[46]
Hf_3AlC_2	349	79	79	283	123	0.963	1.324	161	125	298	1.288	0.192	This
	347	77	80	291	127	0.941	1.251	162	127	302	1.276	0.189	[50]
	357	82	83	283	126	0.940	1.365	166	128	305	1.297	0.193	[51]
	348	79	82	290	112	1.058	1.264	163	121	291	1.347	0.203	[52]
Ta_3AlC_2	411	113	136	343	156	0.772	1.217	214	143	351	1.497	0.227	This
	441	132	138	382	175	0.781	1.217	231	157	384	1.471	0.223	[46]
Ti_3SiC_2	365	89	99	352	156	1.202	1.012	184	143	341	1.287	0.191	[44]
	370	99	111	349	151	1.209	1.038	192	138	334	1.392	0.210	[46]
	372	88	98	353	167	1.267	1.036	185	149	352	1.245	0.183	[48]
	-	-	-	-	-	-	-	185	139	333	1.331	0.20	[49]
	-	-	-	-	-	-	-	186	144	343	1.291	0.192	[48]
Hf_3SiC_2	357	93	115	334	157	1.362	1.005	188	136	329	1.382	0.209	This
	348	101	120	335	144	1.300	0.972	190	127	312	1.496	0.227	[46]
Ta_3SiC_2	335	145	221	325	179	3.284	0.365	239	103	270	2.320	0.317	This
	352	220	210	345	182	2.628	1.126	256	102	270	2.509	0.324	[46]
Zr_3SiC_2	323	85	99	304	135	0.794	1.024	169	122	295	1.385	0.209	This
	320	100	107	296	125	0.804	1.090	174	113	279	-	0.233	[46]
Mo_3SiC_2	377	175	186	364	151	1.637	1.011	245	116	301	2.112	0.300	This
Hf_3SnC_2	320	95	96	300	115	1.075	1.093	168	112	275	1.500	0.227	[45]
	326	96	97	300	107	0.991	1.123	170	110	272	1.550	0.234	[46]
Ti_3SnC_2	319	103	80	304	113	0.976	1.170	163	112	273	1.455	0.221	[44]
	331	96	80	285	108	0.943	1.302	161	113	274	1.436	0.217	[46]
	331	91	81	299	129	1.103	1.193	162	122	285	1.328	0.208	[48]
Zr_3SnC_2	280	92	84	257	110	1.192	1.179	148	99	243	1.495	0.227	[45]
	297	90	87	268	95	0.972	1.177	154	98	244	1.571	0.237	[46]
Ti_3InC_2	338	80	63	276	92	0.754	1.371	151	111	267	1.360	0.205	[44]
	340	85	67	263	97	0.826	1.478	152	111	267	1.362	0.205	[46]
Ti_3GaC_2	359	78	69	292	123	0.959	1.341	159	130	306	1.223	0.179	[44]
	356	86	75	285	113	0.920	1.390	162	122	293	1.324	0.198	[46]
Ti_3GeC_2	356	88	91	324	140	1.125	1.125	175	134	320	1.306	0.195	[44]
	357	100	97	325	129	1.051	1.152	180	126	307	1.426	0.216	[46]
	355	85	94	338	148	1.171	1.032	177	138	312	1.283	0.207	[48]

* Elastic constants and moduli are shown in round figures.

In order to gain information about the brittle or ductile failure of the MAX phases, the Pugh's modulus (B/G) is used [53]. More analytically, when the Pugh's modulus exceeds 1.75, the material is characterized as ductile, which means that a crack progresses slowly when plastic deformation occurs. Conversely, in brittle materials, cracks extend rapidly with little applied stress. According to the results of Table 1, all of the MAX phases studied are brittle, except for Mo_3SiC_2 and Ta_3SiC_2. Another important parameter is the anisotropy factor $k_c/k_a = (c_{11} + c_{12} - 2c_{13})/(c_{33} - c_{13})$, which

indicates whether the MAX phase is more compressible along the a- or c-axis. It is obvious that Ti_3SiC_2, Mo_3SiC_2, Hf_3SnC_2, Hf_3SiC_2, V_3AlC_2, and Ta_3SiC_2 are the only MAX compounds of those studied where compression on the a-axis has almost the same value as on the c-axis.

The Poisson's ratio is another important constant that informs us if the material is a central-force solid or a non-central-force solid [48], and also classifies the materials as brittle or ductile [54,55]. If the Poisson's ratio is between 0.25 and 0.50, then the material is a central-force solid. Otherwise, it is a non-central-force solid. Furthermore, if the Poisson's ratio is more than 0.26, then the solid is ductile, and if it has a lower value, it is brittle. The calculated results show that all the studied MAX phases in Table 1 are non-central-force and brittle, except for Mo_3SiC_2 and Ta_3SiC_2, which are central-force.

The elastic anisotropy, A, is an important description meaning that a body cannot develop the same strain independently of the direction in which the stress is applied. The elastic anisotropy factor indicates how the elastic properties of a solid are dependent on the direction of the stress. Additionally, the elastic anisotropy is connected with the thermal expansion and the crystal microcracks [56]. For the MAX phase systems that are hexagonal, the elastic anisotropy factor is calculated from the equation $A = 4c_{44}/(c_{11} + c_{33} - 2c_{13})$, and if $A = 1$, the crystal is isotropic. The results of Table 1 characterize Mo_3SiC_2 and Ta_3SiC_2 as being more elastically anisotropic than the other MAX phases, and because the value of the elastic anisotropy factor of Hf_3SnC_2 is almost 1, this MAX phase is elastically isotropic.

As regards the elastic properties of the MXenes, focusing on the research of Ge et al. [57] on the superconducting and high hardness of Mo_3C_2, it has been proved that it is a brittle material with a B/G of 2.35. We calculated that the hypothetical Mo_3SiC_2 is a brittle material, and we found that the B/G is slightly lower than the similar MXene, with a value of 2.11. As a result, it is seen that the Mo_3SiC_2 is not as brittle as Mo_3C_2, which makes it more difficult to crack during "diffusion". As regards the Ti_3C_2, Borysiuk et al. [58] used the molecular dynamics method in order to predict the elastic properties of the $Ti_{n+1}C_n$ MXenes, and they calculated, in the case of Ti_3C_2, a value of 502 GPa for the Young's modulus, while Bai calculated a c_{11} constant equal to 523 GPa [59]. Compared to our results, it is evident that for every one of the Ti_3AC_2 MAX compounds, the Young modulus and the elastic constant c_{11} have much lower values. Focusing on the Zr_3C_2 MXene, Xie et al. [60] made a theoretical study on the elastic properties of that MXene, and compared to our 312 MAX phases with Zr-A-C, it is seen that only the Zr_3SnC_2 is less stiff. As a result, it will be softer and more easily machinable than the Zr_3C_2. From all of the above, it is evident that the majority of our MAX phases are performing with better elasticity characteristics and can be more easily manipulated than the similar MXenes, in order to be used as anodes in Li-ion batteries (LIBs).

3.2. Lithiation

The formation energy to incorporate a Li atom in the MAX phase, with ΔH for Li-intercalated systems, is defined by the following equation:

$$\Delta H = E(\text{withxLi}) - E(\text{withoutLi}) - xE(\text{Li}) \quad (2)$$

where *E* (with xLi) and *E* (without Li) are the energies of the system with and without Li atoms. Herein, we used one Li atom as an interstitial, and in result, x = 1. Also, *E* (Li) is the total energy of a single Li atom (here, it is 192.029 eV). In order to calculate the energy of the one Li atom, we performed a calculation for a supercell consisting of 67 Li atoms, and we performed geometry relaxation. We thus calculated the energy of the supercell, and we divided it with 67 in order to find the energy of the one atom. In Table 2, the formation energies of the lithiated 312 MAX phases are provided.

Table 2. The formation energy of 312 MAX phases when one Li atom is inserted.

312 MAX Phases	Formation Energy/eV
Ti_3AlC_2	1.1966
Zr_3AlC_2	0.1499
V_3AlC_2	2.6507
Hf_3AlC_2	0.4172
Ta_3AlC_2	1.7890
Ti_3SiC_2	1.1597
Hf_3SiC_2	0.6902
Ta_3SiC_2	1.2943
Mo_3SiC_2	0.0056
Zr_3SiC_2	0.1608
Hf_3SnC_2	1.9508
Ti_3SnC_2	2.9303
Zr_3SnC_2	1.6645
Ti_3InC_2	2.1320
Ti_3GaC_2	0.9735
Ti_3GeC_2	1.5416

From Table 2, it is evident that the lithiation of the 312 MAX phases studied here is endothermic, which reflects instability. However, Mo_3SiC_2, Hf_3AlC_2, Zr_3AlC_2, and Zr_3SiC_2 exhibit Li formation energies less than 0.5 Ev, making the incorporation of Li in the MAX lattice feasible, and they are even lower than those of MAX materials considered in previous works [61–63]. This is extremely important, as MXenes are generally considered better candidates for battery applications, compared to the MAX phases. Nevertheless, the present work identifies four materials (Mo_3SiC_2, Hf_3AlC_2, Zr_3AlC_2, and Zr_3SiC_2) that are potentially important for such applications. It should be stressed that previous experimental works have only identified oxygen-doped Ti_3SiC_2 as having high Li-ion storage capacity, and hence, as being potentially important as an anode material for Li-ion batteries [64]. In the present study, though, we found that Ti_3SiC_2 has a high formation energy for lithiation (refer to Table 2). This implies that doping could further decrease the Li-intercalation formation energy of Mo_3SiC_2, Hf_3AlC_2, Zr_3AlC_2, and Zr_3SiC_2, thus making them appropriate candidates for battery applications. MAX phases present potential advantages over MXenes, exhibiting better material properties (high thermal-shock resistance, elastic stiffness, melting temperatures, and electrical and thermal conductivity). They are less-complicated structures, as they do not need functional groups to be stabilized [61]. We searched the literature about the formation energy of similar lithiated MXene structures, but we could only find a report about Ti_3C_2 where the formation energy for the lithiated structure was calculated at 4.40 eV [65]. It is obvious that this value is higher than our theoretical results, so the lithiation in the 312 MAX phases needs less energy than the above-mentioned MXene.

In an effort to link the elastic properties with the Li formation energies in the 312 MAX phases, we considered Figure 3. This was motivated by initial work on the Ti_3AC_2 (A = Sn, Si, Ge, Ga, Al, and In) MAX phases where there is a decrease of Li formation energy with respect to the C_{11} elastic constant (refer to Figure 3a). Nevertheless, when considering the whole range of the 312 MAX phases, there is no specific trend (refer to Figure 3b–d). Future theoretical work should include thermodynamic models to investigate further if the bulk properties impact the formation energies of Li in these systems [66–68].

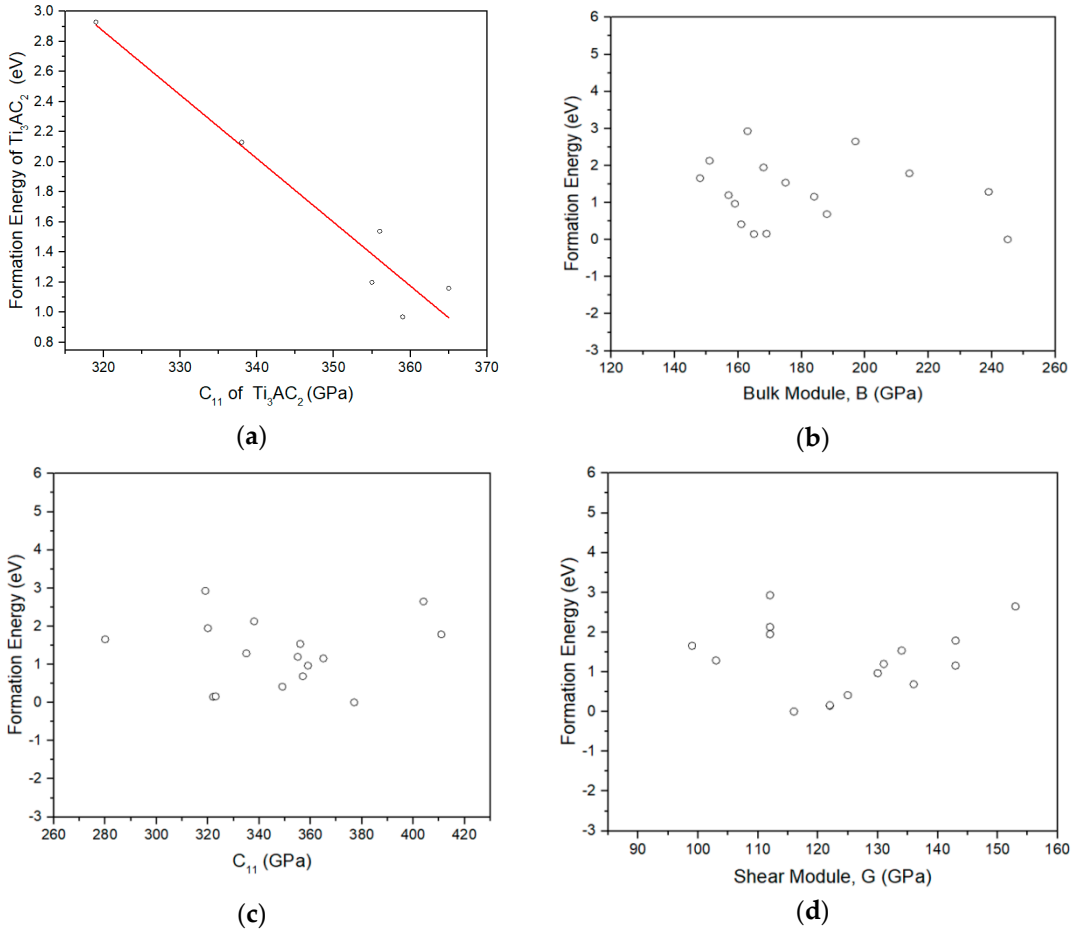

Figure 3. (**a**) The dependence of the Li MAX phases formation energy (eV), with respect to the c_{11} (GPa) elastic constant for the Ti_3AC_2 (A = Sn, Si, Ge, Ga, Al, In) MAX phases. (**b**) The dependence of the formation energy (eV) of lithiated 312 MAX phases from the bulk modulus (GPa). (**c**) The dependence of the formation energy (eV) of the lithiated 312 MAX phases from the C_{11} (GPa) elastic constant. (**d**) The dependence of the formation energy (eV) of the lithiated 312 MAX phases from the shear modulus G (GPa).

4. Conclusions

To summarize, the mechanical behavior and the formation energy for the lithiation of the 312 MAX phases has been calculated using the density functional theory. From our calculations, it is evident that Zr_3SnC_2 is more prone to shape change along the b- and c-axes when stress along the a-axis is applied. Moreover, Zr_3SnC_2 does not need high stress in order to deform, and has low resistance to deformation under compression.

The energy to incorporate Li-ions in the 312 MAX phases is considerably high, with the exception of Mo_3SiC_2, Hf_3AlC_2, Zr_3AlC_2, and Zr_3SiC_2, for which formation energies of Li intercalation less than 0.5 eV were calculated. The Li formation energies in Mo_3SiC_2 and Zr_3SiC_2 are particularly low. However, they have not yet been synthesized. Regarding the other compounds, it could be proposed that their potential as LIBs or supercapacitor anodes should be examined.

To conclude, from the four 312 materials that we propose should be examined for potential lithiation, two of them have already been synthesized in stable forms (Zr_3SnC_2 and Hf_3AlC_2) and one has been synthesized as part of a mixed structure (Zr_3SiC_2), and so we believe that their lithiation ability could be investigated both experimentally and theoretically. There have been, compared to the MXenes, very few studies of the MAX phases for battery applications. Obviously, the incorporation of Li is only part of the picture, and future studies should focus on the diffusion of Li from both an

experimental and theoretical viewpoint. Doping strategies should also be employed to lower the formation and migration energies of Li in the MAX phases.

Author Contributions: Conceptualization, A.C.; formal analysis, P.P.F. and M.A.H.; investigation, P.P.F., S.-R.G.C., A.K. and N.K.; writing—original draft preparation, P.P.F. and A.C.; writing—review and editing, M.E.F. and M.V.; supervision, M.V. and A.C.

Funding: This research received no external funding.

Acknowledgments: P.P.F., S.-R.G.C., A.C., N.K. and M.E.F. are grateful for funding from the Lloyd's Register Foundation, a charitable foundation helping to protect life and property by supporting engineering-related education, public engagement, and the application of research.

Conflicts of Interest: The authors declare no conflicts of interest.

References

1. Barsoum, M.W.; El-Raghy, T. The MAX phases: Unique new carbide and nitride materials: Ternary ceramics turn out to be surprisingly soft and machinable, yet also heat-tolerant, strong and lightweight. *Am. Sci.* **2001**, *89*, 334–343. [CrossRef]
2. Barsoum, M.W. The $M_{N+1}AX_N$ phases: A new class of solids: Thermodynamically stable nanolaminates. *Prog. Solid State Chem.* **2000**, *28*, 201–281. [CrossRef]
3. Chen, H.; Yang, D.; Zhang, Q.; Jin, S.; Guo, L.; Deng, J.; Chen, X. A series of MAX phases with MA-triangular-prism bilayers and elastic properties. *Angew. Chem.* **2019**, *131*, 4624–4628. [CrossRef]
4. Thore, A.; Rosén, J. An investigation of the in-plane chemically ordered atomic laminates $(Mo_{2/3}\ Sc_{\ 1/3})_2$ AlC and $(Mo_{2/3}\ Y_{1/3})_2$ AlC from first principles. *Phys. Chem. Chem. Phys.* **2017**, *19*, 21595–21603. [CrossRef]
5. Nowotny, H. Strukturchemieeinigerverbindungen der übergangsmetallemit den elementen C, Si, Ge, Sn. *Prog. Solid State Chem.* **1971**, *5*, 27–70. [CrossRef]
6. Barsoum, M.W.; El-Raghy, T. Synthesis and characterization of a remarkable ceramic. *J. Am. Ceram. Soc.* **1996**, *79*, 1953. [CrossRef]
7. Khazaei, M.; Ranjbar, A.; Esfarjani, K.; Bogdanovski, D.; Dronskowski, R.; Yunoki, S. Insights into exfoliation possibility of MAX phases to MXenes. *Phys. Chem. Chem. Phys.* **2018**, *20*, 8579–8592. [CrossRef]
8. Barsoum, M.W. *MAX Phases: Properties of Machinable Ternary Carbides and Nitrides*; John Wiley & Sons: Hoboken, NJ, USA, 2013.
9. Eklund, P.; Rosen, J.; Persson, P.O.Å. Layered ternary $M_{n+1}AX_n$ phases and their 2D derivative MXene: An overview from a thin-film perspective. *J. Phys. D Appl. Phys.* **2017**, *50*, 113001. [CrossRef]
10. Buschow, K.J.; Cahn, R.W.; Flemings, M.C.; Ilschner, B.; Kramer, E.J.; Mahajan, S. *Encyclopedia of Materials Science and Technology*; Elsevier: Amsterdam, The Netherlands, 2001.
11. Sun, Z.M. Progress in research and development on MAX phases: A family of layered ternary compounds. *Int. Mater. Rev.* **2011**, *56*, 143–166. [CrossRef]
12. Wang, X.H.; Zhou, Y.C. Layered machinable and electrically conductive Ti_2AlC and Ti_3AlC_2 ceramics: A review. *J. Mater. Sci. Tehnol.* **2011**, *26*, 385–416. [CrossRef]
13. Middleburgh, S.C.; Lumpkin, G.R.; Riley, D. Accommodation, accumulation, and migration of defects in Ti_3SiC_2 and Ti_3AlC_2 MAX phases. *J. Am. Ceram. Soc.* **2013**, *96*, 3196–3201.
14. Sokol, M.; Natu, V.; Kota, S.; Barsoum, M.W. On the chemical diversity of the MAX phases. *Trends Chem.* **2019**, *1*, 210. [CrossRef]
15. Horlait, D.; Grasso, S.; Chroneos, A.; Lee, W.E. Attempts to synthesise quaternary MAX phases $(Zr,M)_2AlC$ and $Zr_2(Al,A)C$ as a way to approach Zr_2AlC. *Mater. Res. Lett.* **2016**, *4*, 137–144. [CrossRef]
16. Horlait, D.; Grasso, S.; Al Nasiri, N.; Burr, P.A.; Lee, W.E. Synthesis and high-temperature oxidation of MAX phases in the Cr-Ti-Al-C quaternary system. *J. Am. Ceram. Soc.* **2016**, *99*, 682–690. [CrossRef]
17. Saltas, V.; Horlait, D.; Sgourou, E.N.; Vallianatos, F.; Chroneos, A. Modelling solid solutions with cluster expansion, special quasirandom structures, and thermodynamic approaches. *Appl. Phys. Rev.* **2017**, *4*, 041301. [CrossRef]
18. Horlait, D.; Middleburgh, S.C.; Chroneos, A.; Lee, W.E. Synthesis and DFT investigation of new bismuth-containing MAX phases. *Sci. Rep.* **2016**, *6*, 18829. [CrossRef]

19. Lapauw, T.; Halim, J.; Lu, J.; Cabioc'h, T.; Hultman, L.; Barsoum, M.W.; Lambrinou, K.; Vleugels, J. Synthesis of the novel Zr_3AlC_2 MAX phase. *J. Eur. Ceram. Soc.* **2016**, *36*, 943–947. [CrossRef]
20. Talapatra, A.; Duong, T.; Son, W.; Gao, H.; Radovic, M.; Arróyave, R. High-throughput combinatorial study of the effect of M site alloying on the solid solution behavior of M_2AlC MAX phases. *Phys. Rev. B* **2016**, *94*, 104106. [CrossRef]
21. Tunca, B.; Lapauw, T.; Karakulina, O.M.; Batuk, M.; Cabioc'h, T.; Hadermann, J.; Delville, R.; Lambrinou, K.; Vleugels, J. Synthesis of MAX phases in the Zr-Ti-Al-C system. *Inorg. Chem.* **2017**, *56*, 3489–3498. [CrossRef]
22. Arróyave, R.; Talapatra, A.; Duong, T.; Son, W.; Gao, H.; Radovic, M. Does aluminium play well with others? Intrinsic Al-A alloying behavior in 211/312 MAX phases. *Mater. Res. Lett.* **2017**, *5*, 170–178.
23. Hadi, M.A.; Panayiotatos, Y.; Chroneos, A. Structural and optical properties of the recently synthesized $(Zr_3$-xTix)AlC_2 MAX phases. *J. Mater. Sci. Mater. Electron.* **2017**, *28*, 3386–3393. [CrossRef]
24. Lei, J.C.; Zhang, X.; Zhou, Z. Recent advances in MXene: Preparation, properties, and applications. *Front. Phys.* **2015**, *10*, 276–286. [CrossRef]
25. Zapata-Solvas, E.; Hadi, M.A.; Horlait, D.; Parfitt, D.C.; Thibaud, A.; Chroneos, A.; Lee, W.E. Synthesis and physical properties of $(Zr_{1-x}Ti_x)AlC_2$ MAX phases. *J. Am. Ceram. Soc.* **2017**, *100*, 3393–3401. [CrossRef]
26. Kim, H.; Park, K.Y.; Hong, J.; Kang, K. All-graphene-battery: Bridging the gap between supercapacitors and lithium ion batteries. *Sci. Rep.* **2014**, *4*, 5278. [CrossRef]
27. Naguib, M.; Come, J.; Dyatkin, B.; Presser, V.; Taberna, P.L.; Simon, P.; Barsoum, M.W.; Gogotsi, Y. MXene: A promising transition metal carbide anode for lithium-ion batteries. *Electrochem. Commun.* **2012**, *16*, 61–64. [CrossRef]
28. Liang, X.; Garsuch, A.; Nazar, L.F. Sulfur cathodes based on conductive MXene nanosheets for high-performance lithium–sulfur batteries. *Angew. Chem.* **2015**, *54*, 3907–3911. [CrossRef]
29. Khazaei, M.; Arai, M.; Sasaki, T.; Chung, C.Y.; Venkataramanan, N.S.; Estili, M.; Sakka, Y.; Kawazoe, Y. Novel electronic and magnetic properties of two-dimensional transition metal carbides and nitrides. *Adv. Funct. Mater.* **2013**, *23*, 2185–2192. [CrossRef]
30. Peer Mohamed, A. Shear induced micromechanical synthesis of Ti_3SiC_2 MAXene nanosheets for functional applications. *RSC Adv.* **2015**, *5*, 51242–51247.
31. Zhou, J.; Zha, X.; Chen, F.Y.; Ye, Q.; Eklund, P.; Du, S.; Huang, Q. A two-dimensional zirconium carbide by Selective etching of Al_3C_3 from nanolaminated $Zr_3Al_3C_5$. *Angew. Chem.* **2016**, *55*, 5008–5013. [CrossRef]
32. Zapata-Solvas, E.; Christopoulos, S.R.G.; Ni, N.; Parfitt, D.C.; Horlait, D.; Fitzpatrick, M.E.; Chroneos, A.; Lee, W.E. Experimental synthesis and density functional theory investigation of radiation tolerance of Zr3 $(Al_{1-x}S\ i_x)\ C_2$ MAX phases. *J. Am. Ceram. Soc.* **2017**, *100*, 1377–1387. [CrossRef]
33. Farle, A.M.; Van der Zwaag, S.; Sloof, W.G. A conceptual study into the potential of max-phase ceramics for self-healing of crack damage. In Proceedings of the 4th International Conference on Self-Healing Materials, ICSHM 2013, Ghent, Belgium, 16–20 June 2013.
34. Lapauw, T.; Tunca, B.; Cabioc'h, T.; Lu, J.; Persson, P.O.A.; Lambrinou, K.; Vleugels, J. Synthesis of MAX phases in the Hf–Al–C system. *Inorg. Chem.* **2016**, *55*, 10922–10927. [CrossRef]
35. Pshyk, A.V.; Coy, E.; Kempiński, M.; Scheibe, B.; Jurga, S. Low-temperature growth of epitaxial Ti_2AlC MAX phase thin films by low-rate layer-by-layer PVD. *Mater. Res. Let.* **2019**, *7*, 244–250. [CrossRef]
36. Siebert, J.P.; Bischoff, L.; Lepple, M.; Zintler, A.; Molina-Luna, L.; Wiedwald, U.; Birkel, C.S. Sol–gel based synthesis and enhanced processability of MAX phase Cr $_2$ GaC. *J. Mater. Chem. C* **2019**, *7*, 6034–6040. [CrossRef]
37. Payne, M.C.; Teter, M.P.; Allan, D.C.; Arias, T.A.; Joannopoulos, J.D. Iterative minimization techniques for ab initio total-energy calculations: Molecular dynamics and conjugate gradients. *Rev. Mod. Phys.* **1992**, *64*, 1045. [CrossRef]
38. Segall, M.D.; Lindan, P.J.; Probert, M.A.; Pickard, C.J.; Hasnip, P.J.; Clark, S.J.; Payne, M.C. First-principles simulation: Ideas, illustrations and the CASTEP code. *J. Phys. Condens. Matter.* **2002**, *14*, 2717. [CrossRef]
39. Perdew, J.; Burke, K.; Ernzerhof, M. Generalized gradient approximation made simple. *Phys. Rev. Lett.* **1996**, *77*, 3865. [CrossRef]
40. Vanderbilt, D. Soft self-consistent pseudopotentials in a generalized eigenvalue formalism. *Phys. Rev. B* **1990**, *41*, 7892. [CrossRef]
41. Monkhorst, H.J.; Pack, J.D. Special points for Brillouin-zone integrations. *Phys. Rev. B* **1976**, *13*, 5188. [CrossRef]

42. Barsoum, M.W. The $M_{n+1}AX_n$ phases and their properties. In *Ceramics Science and Technology*; Riedel, R.R., Chen, I.W., Eds.; Wiley-VCH Verlag GmbH & Co: Weinheim, Germany, 2010; Volume 2.
43. Born, M. On the stability of crystal lattices. In *Mathematical Proceedings of the Cambridge Philosophical Society*; Cambridge University Press: Cambridge, UK, 1940; Volume 36, pp. 160–172.
44. Christopoulos, S.R.; Filippatos, P.P.; Hadi, M.A.; Kelaidis, N.; Fitzpatrick, M.E.; Chroneos, A. Intrinsic defect processes and elastic properties of Ti_3AC_2 (A= Al, Si, Ga, Ge, In, Sn) MAX phases. *J. Appl. Phys.* **2018**, *123*, 025103. [CrossRef]
45. Hadi, M.A.; Christopoulos, S.R.; Naqib, S.H.; Chroneos, A.; Fitzpatrick, M.E.; Islam, A.K.M.A. Physical properties and defect processes of M_3SnC_2 (M = Ti, Zr, Hf) MAX phases: Effect of M-elements. *J. Alloy. Comp.* **2018**, *748*, 804–813. [CrossRef]
46. Aryal, S.; Sakidja, R.; Barsoum, M.W.; Ching, W.Y. A genomic approach to the stability, elastic, and electronic properties of the MAX phases. *Phys. Status Solidi B* **2014**, *251*, 1480–1497. [CrossRef]
47. Ali, M.S.; Islam, A.K.M.A.; Hossain, M.M.; Parvin, F. Phase stability, elastic, electronic, thermal and optical properties of $Ti_3Al_{1-x}Si_xC_2$ ($0 \leq \times \leq 1$): First principle study. *Phys. B* **2012**, *407*, 4221–4228. [CrossRef]
48. Wang, W.; Sun, L.; Yang, Y.; Dong, J.; Gu, Z.; Jin, H. Pressure effects on electronic, anisotropic elastic and thermal properties of Ti_3AC_2 (Si, Ge and Sn) by ab initio calculations. *Results Phys.* **2017**, *7*, 1055–1065. [CrossRef]
49. Finkel, P.; Barsoum, M.W.; El-Raghy, T. Low temperature dependencies of the elastic properties of Ti_4AlN_3, Ti_3 $Al_{1.1}$ $C_{1.8}$, and Ti_3SiC_2. *J. Appl. Phys.* **2000**, *87*, 1701–1703. [CrossRef]
50. Roknuzzaman, M.; Hadi, M.A.; Ali, M.A.; Hossain, M.M.; Jahan, N.; Uddin, M.M.; Alarco, J.A.; Ostrikov, K. First hafnium-based MAX phase in the 312 family, Hf_3AlC_2: A first principles study. *J. Alloy Compd.* **2017**, *727*, 616–626. [CrossRef]
51. He, X.; Bai, Y.; Zhu, C.; Sun, Y.; Li, M.; Barsoum, M.W. General trends in the structural, electronic and elastic properties of the M_3AlC_2 phases ($M\frac{1}{4}$ transition metal): A first-principle study. *Comput. Mater. Sci.* **2010**, *49*, 691–698. [CrossRef]
52. Radovic, M.; Barsoum, M.W.; Ganguly, A.; Zhen, T.; Finkel, P.; Kalidindi, S.R.; Lara-Curzio, E. On the elastic properties and mechanical damping of Ti_3SiC_2, Ti_3GeC_2, $Ti_3Si_{0.5}Al_{0.5}C_2$ and Ti_2AlC in the 300–1573 K temperature range. *Acta Mater.* **2006**, *54*, 2757–2767. [CrossRef]
53. Pugh, S.F. Relations between the elastic moduli and the plastic properties of polycrystalline pure metals. *Philos. Mag.* **1954**, *45*, 823–843. [CrossRef]
54. Anderson, O.L.; Demarest, H.H., Jr. Elastic constants of the central force model for cubic structures: Polycrystalline aggregates and instabilities. *J. Geophy. Res.* **1971**, *76*, 1349–1369. [CrossRef]
55. Frantsevich, I.N.; Voronov, F.F.; Bokuta, S.A. *Elastic Constants and Elastic Moduli of Metals and Insulators*; Frantsevich, I.N., Ed.; NaukovaDumka: Kiev, Ukraine, 1983; Volume 60, p. 180.
56. Vaitheeswaran, G.; Kanchana, V.; Svane, A.; Delin, A. Elastic properties of MgCNi3—A superconducting perovskite. *J. Phys. Condens. Matter.* **2007**, *19*, 326214. [CrossRef]
57. Ge, Y.; Ma, S.; Bao, K.; Tao, Q.; Zhao, X.; Feng, X.; Li, L.; Liu, B.; Zhu, P.; Cui, T. Superconductivity with high hardness in Mo_3 C_2. *Inorg. Chem. Front.* **2019**, *6*, 1282–1288. [CrossRef]
58. Borysiuk, V.N.; Mochalin, V.N.; Gogotsi, Y. Molecular dynamic study of the mechanical properties of two-dimensional titanium carbides $Ti_{n+1}C_n$ (MXenes). *Nanotechnology* **2015**, *26*, 265705. [CrossRef]
59. Bai, Y.; Zhou, K.; Srikanth, N.; Pang, J.H.; He, X.; Wang, R. Dependence of elastic and optical properties on surface terminated groups in two-dimensional MXene monolayers: A first-principles study. *RSC Adv.* **2016**, *6*, 35731–35739. [CrossRef]
60. Xie, C.; Oganov, A.R.; Li, D.; Debela, T.T.; Liu, N.; Dong, D.; Zeng, Q. Effects of carbon vacancies on the structures, mechanical properties, and chemical bonding of zirconium carbides: A first-principles study. *Phys. Chem. Chem. Phys.* **2016**, *18*, 12299–12306. [CrossRef]
61. Zhu, J.J.; Chroneos, A.; Eppinger, J.; Schwingenschlögl, U. S-functionalized MXenes as electrode materials for Li-ion batteries. *Appl. Mater. Today* **2016**, *5*, 19–24. [CrossRef]
62. Zhu, J.; Chroneos, A.; Wang, L.; Rao, F.; Schwingenschloegl, U. Stress-enhanced lithiation in MAX compounds for battery applications. *Appl. Mater. Today* **2017**, *9*, 192–195. [CrossRef]
63. Pang, J.B.; Mendes, R.G.; Bachmatiuk, A.; Zhao, L.; Ta, H.Q.; Gemming, T.; Liu, H.; Liu, Z.F.; Rummeli, M.H. Applications of 2D MXenes in energy conversion and storage systems. *Chem. Soc. Rev.* **2019**, *48*, 72–133. [CrossRef]

64. Luan, S.R.; Zhou, J.S.; Xi, Y.K.; Han, M.Z.; Wang, D.; Gao, J.J.; Hou, L.; Gao, F.M. High lithium-ion storage performance of Ti_3SiC_2 MAX by oxygen doping. *Chem. Sel.* **2019**, *4*, 5319–5321.
65. Er, D.; Li, J.; Naguib, M.; Gogotsi, Y.; Shenoy, V.B. Ti_3C_2 MXene as a high capacity electrode material for metal (Li, Na, K., Ca) ion batteries. *ACS Appl. Mater. Interfaces* **2014**, *6*, 11173–11179. [CrossRef]
66. Varotsos, P. Point defect parameters in β-PbF_2 revisited. *Solid State Ion.* **2008**, *179*, 438–441. [CrossRef]
67. Chroneos, A.; Vovk, R.V. Modeling self-diffusion in UO_2 and ThO_2 by connecting point defect parameters with bulk properties. *Solid State Ion.* **2015**, *274*, 1–3. [CrossRef]
68. Cooper, M.W.D.; Grimes, R.W.; Fitzpatrick, M.E.; Chroneos, A. Modeling oxygen self-diffusion in UO_2 under pressure. *Solid State Ion.* **2015**, *282*, 26–30. [CrossRef]